Hybrid Cable Thruster Actuated Remotely Operated Underwater Vehicle

Youssef Attia, Enrico Simetti, Marc Gouttefarde

Hybrid Cable Thruster Actuated Remotely Operated Underwater Vehicle

Youssef Attia * **Enrico Simetti** *,** **Marc Gouttefarde** ***

* *Università degli Studi di Genova, via all'Opera Pia 13, 16145 Genova, Italy (e-mail: s5171925@studenti.unige.it).*
** *Interuniversity Research Center on Integrated Systems for the Marine Environment, via all'Opera Pia 13, 16145 Genova, Italy (e-mail: enrico.simetti@unige.it)*
*** *LIRMM, Univ Montpellier, CNRS, Montpellier, France (e-mail: marc.gouttefarde@lirmm.fr)*

Abstract: This paper introduces a novel Hybrid Cable Thruster Actuated Remotely Operated Underwater Vehicle (HCT-ROV), merging the strengths of ROVs and Cable-Driven Parallel Robots for enhanced underwater capabilities. It presents the world's first HCT-ROV prototype, together with a control law using Quadratic Programming (QP) for efficient operation. Extensive MATLAB simulations and prototype tests demonstrate superior performance in tasks like object transportation. This research work paves the way for advanced underwater exploration and operations, emphasizing the need for further optimization in real-world applications.

Keywords: HCT-ROV, ROV, CDPR, Control Allocation, Quadratic Programming.

1. INTRODUCTION

Approximately 71% of Earth's surface is enveloped by water, revealing a vast, resource-rich underwater world. Traditionally, human divers and submersibles were key for underwater exploration, yet faced depth limitations and risks. Divers are typically restricted to around 50 (m), constraining the scope of underwater operations. Submersibles, like Victor Vescovo's record-breaking 10,934 (m) descent, broadened exploration but were costly and risky, leading to rise of underwater robotics.

Despite Remotely Operated Underwater Vehicles (ROVs) advancements in underwater missions, their limitations, such as lift force, power consumption, and high operation costs, necessitate alternatives. ROVs depend on surface support, specialized crews, and operators, with daily costs up to (50k€) Simetti (2020); Cieślak et al. (2020). These constraints are pronounced in heavy payload tasks or prolonged station keeping, requiring larger, pricier ROVs. Cable-Driven Parallel Robots (CDPRs) present a viable solution to these challenges.

CDPRs are defined by Gouttefarde and Bruckmann (2022) as "dexterous lifting machines using several cables to avoid, at least partially, payload sway." These robots comprise a support structure, winches, and a mobile platform, allowing precise control of the platform position and orientation. An exemplary application of CDPRs is the MAELSTROM project Gouttefarde et al. (2023), where a CDPR mobile platform, equipped with a gripper and suction system, successfully collected seabed litter in Italy's Venice Lagoon in 2022 see Fig. 1.

CDPRs offer a solution to ROV limitations like limited lift force. Insights from the MAELSTROM project, which

Fig. 1. The MAELSTROM project's CDPR engaged in underwater litter removal: A detailed view of the mechanism, cable control from the floating barge, and litter extraction in action in the Venice's lagoon, Italy, 2022. Gouttefarde et al. (2023).

pioneered the first underwater CDPR, pave the way for hybrid systems combining ROV and CDPR strengths.

The concept of Hybrid Cable Thruster Actuated Remotely Operated Underwater Vehicles (HCT-ROVs) was initially introduced by El-Ghazaly et al. (2015), focusing on the kinematic and dynamic modeling of a hybrid cable-thruster actuated underwater vehicle-manipulator system (HCT-UVMS). This early work emphasized enhanced force capabilities over traditional ROVs.

Further research, particularly by Sacchi et al. (2022), built on these insights, presenting a comprehensive control architecture and algorithm for HCT-ROV. Validated through Vortex Studio simulations, this research showcased HCT-ROV efficiency in lifting heavy payloads, surpassing traditional ROVs.

The authors, however, pointed out areas for future exploration, such as the impact of environmental factors,

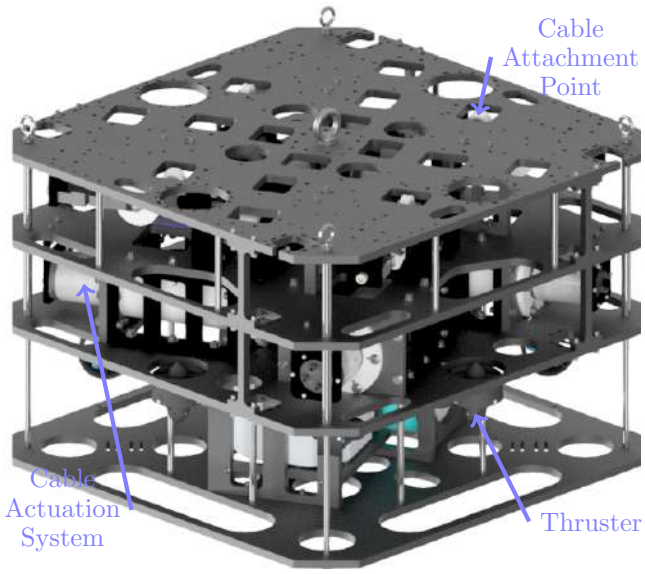

Fig. 2. The first HCT-ROV prototype and its main components (Eight T200 Thrusters and Four Cable Actuation Systems.)

performance with varying underwater vehicle sizes, and advanced control system development. The goal is to progress from simulations to real-world applications and here is where the first HCT-ROV prototype can be seen in Fig. 2.

1.1 Contributions of This Paper

This paper aims to build upon the initial development of the HCT-ROV and makes the following contributions.

- **Forward and Inverse Kinetostatic models:** The development and implementation of a novel forward and inverse Kinetostatics, utilizing quadratic programming (QP) for efficient control allocation in the overactuated HCT-ROV prototype system.
- **Simulation-Based Validation:** Extensive validation of the proposed kinetostatics modeling and control allocation through developed MATLAB simulations applied to a novel HCT-ROV prototype in various scenarios.

2. MODELING AND CONTROL LAW

As shown in Fig. 3, the vehicle frame ν in the world frame ω is represented by the configuration $\boldsymbol{\gamma} = [\boldsymbol{\gamma}_1\ \boldsymbol{\gamma}_2]^\top \in \mathbb{R}^6$, with position $\boldsymbol{\gamma}_1 = [X, Y, Z]^\top$ and roll-pitch-yaw (RPY) orientation $\boldsymbol{\gamma}_2 = [\Phi, \theta, \Psi]^\top$. The vehicle rotation matrix is ${}^{\omega}_{\nu}R = R_Z(\Psi)R_Y(\theta)R_X(\Phi)$. Additionally, cable i connects drawing point B_i on the vehicle to attachment point A_i, with position vectors $\boldsymbol{b}_i$ and $\boldsymbol{a}_i$ relative to frames ν and ω, respectively. The thrusters, attached at points C_i on the vehicle, have position vectors $\boldsymbol{c}_i$ relative to frame ν.

The dynamic behavior of the HCT-ROV is characterized by the following dynamic equation:

$$\boldsymbol{M}\dot{\boldsymbol{\nu}}_r + \boldsymbol{C}(\boldsymbol{\nu}_r)\boldsymbol{\nu}_r + \boldsymbol{D}(\boldsymbol{\nu}_r)\boldsymbol{\nu}_r + \boldsymbol{g}(\boldsymbol{\gamma}) = \boldsymbol{\tau}_a + \boldsymbol{\tau}_{\text{ext}} \quad (1)$$

where $\boldsymbol{M} \in \mathbb{R}^{6\times6}$ represents the total inertia matrix, including both rigid body and added mass effects. The Coriolis and centripetal matrix $\boldsymbol{C}(\boldsymbol{\nu}_r) \in \mathbb{R}^{6\times6}$ and the damping matrix $\boldsymbol{D}(\boldsymbol{\nu}_r) \in \mathbb{R}^{6\times6}$ account for dynamic fluid interactions. The gravity and buoyancy force vector $\boldsymbol{g}(\boldsymbol{\gamma}) \in \mathbb{R}^6$, the actuation wrenches, including both cables and thrusters, $\boldsymbol{\tau}_a \in \mathbb{R}^6$, and the external disturbance forces $\boldsymbol{\tau}_{\text{ext}} \in \mathbb{R}^6$ are involved in this model. Finally, the relative velocity is denoted $\boldsymbol{\nu}_r \in \mathbb{R}^6$ and its rate of change $\dot{\boldsymbol{\nu}}_r \in \mathbb{R}^6$, representing the acceleration.

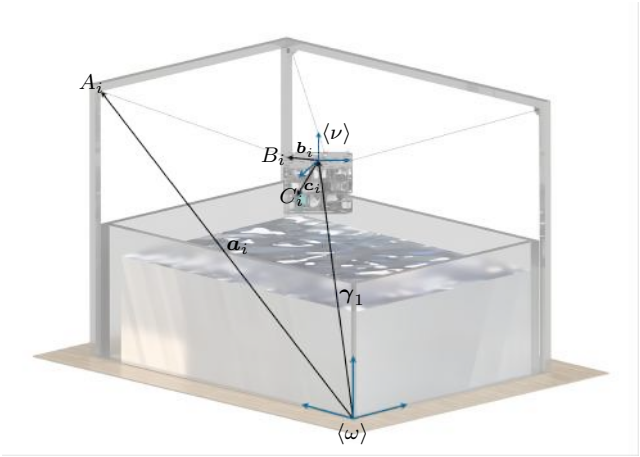

Fig. 3. HCT-ROV kinematic model schematic representation

2.1 Forward Kinematics

This section aims to find the HCT-ROV position and orientation ($\boldsymbol{\gamma}$) for a given cable lengths ($\boldsymbol{\ell}$).

Fig. 4. Under-determined Forward kinematics problem

Similarly to most parallel robots, the forward kinematics of CDPRs is complex. Assuming fixed points A_i in space, and neglecting cable mass and elasticity, the cable length can be expressed as:

$$\ell_i = \left\|\overrightarrow{A_iB_i}\right\| = \left\|(\boldsymbol{\gamma_1} + {}^{\omega}_{\nu}\mathbf{b}_i - \mathbf{a}_i)\right\|, \quad i = 1, 2, \ldots, m \quad (2)$$

For more cables (m) than degrees of freedom (DOFs) ($n = 6$), this forms an over-determined system, and for $m < n$, an under-determined one.

The HCT-ROV prototype has fewer cables ($m = 4$) than DOFs ($n = 6$), making it under-determined. Fixing two DOF (position or angles) converts it into a square system.

Fig. 5. Determined forward kinematics problem

Alternatively, the under-determined system (fig.4) can be solved using optimization methods. The problem can be formulated as follows:

$$\min_{\boldsymbol{\gamma}_a} f(\boldsymbol{\gamma}) = \|e(\boldsymbol{\gamma})\|_2^2 \quad (3)$$

Here, $e(\boldsymbol{\gamma})$ denotes the error between desired cable lengths (ℓ_d) and actual cable lengths (ℓ_a). Note that ℓ_a depends on the HCT-ROV pose ($\boldsymbol{\gamma}_a$), cable tensions (t_a), and thruster forces (f_a). A nonlinear least-square solver [1] can solve this

[1] `https://fr.mathworks.com/help/optim/ug/lsqnonlin.html`

minimization problem. However, certain vehicle poses may cause slack cables, leading to pendulum-like behavior. This necessitates revisiting initial assumptions and examining the HCT-ROV dynamic model Equation (1).

Extensive research has addressed such kinetostatic problem of under-constrained CDPRs. In 2013, Carricato and Merlet (2013) introduced an algorithm for static equilibrium stability using a constrained optimization and linear algebra routines, showing improvement over previous methods. This work validated the effectiveness for a two-cable CDPR. In 2015, Abbasnejad and Carricato (2015) used algebraic equations to derive a least-degree univariate polynomial for any cable number, offering an efficient method alternative. The DGP-Solver software package was utilized for numerical computation, considering solutions with slack cables and integrating stability analysis. Their findings indicated multiple equilibria and control capacity loss due to slack cables. Idà et al. (2019), in 2019, explored the rest-to-rest Trajectory Planning (TP) problem, proposing a technique for accurate path tracking while addressing the kinetostatic relationship. Despite successful experiments with their prototype, dynamic modeling elements like cable elasticity and acceleration were omitted. Recently in 2021, Mishra and Caro (2021) approached the forward kinetostatic problem using an unsupervised neural network, reporting precision and speed surpassing MATLAB's "lsqnonlin" function.

However, these studies focused on the cable components, and non discussed the concept of incorporating thrusters as force generators. Given the complexity of dynamic modeling in early development stages, factors such as vehicle inertia, Coriolis and centripetal effects, and damping coefficients can be initially neglected, with a focus on the static equilibrium of the HCT-ROV.

2.2 HCT-ROV static equilibrium

To maintain the HCT-ROV in a state of static equilibrium, the sum of all forces and moments exerted on the body must be zero. As such, integrating these principles allows modeling the static equilibrium of the HCT-ROV as follows:

$$W_c \boldsymbol{t} + W_t \boldsymbol{f} = \boldsymbol{w}_e \tag{4}$$

where W_c and W_t are the cables and thrusters wrench matrices respectively while $\boldsymbol{t}$ and $\boldsymbol{f}$ are the cable tensions and thruster forces vectors, respectively. $\boldsymbol{w}_e$ is the external wrench, due to gravity and buoyancy effect. The matrices are defined as follows:

$$W_c = \begin{bmatrix} \hat{\boldsymbol{u}}_1 & \hat{\boldsymbol{u}}_2 & \cdots & \hat{\boldsymbol{u}}_m \\ {}^{B_1}_{v}\boldsymbol{b}_1 \times \hat{\boldsymbol{u}}_1 & {}^{B_2}_{v}\boldsymbol{b}_2 \times \hat{\boldsymbol{u}}_2 & \cdots & {}^{B_m}_{v}\boldsymbol{b}_m \times \hat{\boldsymbol{u}}_m \end{bmatrix}_{6\times m} \tag{5}$$

$$W_t = \begin{bmatrix} \hat{\boldsymbol{v}}_1 & \hat{\boldsymbol{v}}_2 & \cdots & \hat{\boldsymbol{v}}_p \\ {}^{C_1}_{v}\boldsymbol{c}_1 \times \hat{\boldsymbol{v}}_1 & {}^{C_2}_{v}\boldsymbol{c}_2 \times \hat{\boldsymbol{v}}_2 & \cdots & {}^{C_p}_{v}\boldsymbol{c}_p \times \hat{\boldsymbol{v}}_p \end{bmatrix}_{6\times p} \tag{6}$$

where $\hat{\boldsymbol{u}} \in \mathbb{R}^3$ and $\hat{\boldsymbol{v}} \in \mathbb{R}^3$ are the unit vectors representing the direction of forces generated by the corresponding cable or thruster, respectively. $\hat{\boldsymbol{v}}$ depends on the thrusters configuration, while $\hat{\boldsymbol{u}}$ is defined as

$$\hat{\boldsymbol{u}}_i = \frac{\overrightarrow{B_i A_i}}{\left|\overrightarrow{B_i A_i}\right|} = \frac{\boldsymbol{a_i} - {}^{\omega}_{\nu}\boldsymbol{b_i} + \boldsymbol{\gamma}_1}{|\boldsymbol{a_i} - {}^{\omega}_{\nu}\boldsymbol{b_i} + \boldsymbol{\gamma}_1|}. \tag{7}$$

The cable tensions ($\boldsymbol{t}$) and thruster forces ($\boldsymbol{f}$) are subject to physical constraints and are defined as:

$$\boldsymbol{t} = [t_1 \ t_2 \ \cdots \ t_m]^{\top}_{1\times m}, \quad 0 \le t_{\min} < t_i < t_{\max} \tag{8}$$

$$\boldsymbol{f} = [f_1 \ f_2 \ \cdots \ f_p]^{\top}_{1\times p}, \quad f_{\min} < f_i < f_{\max} \tag{9}$$

2.3 Forward Kinetostatics

Building on the cable length equation (2) and the static equilibrium equation (4), it is clear that determining the HCT-ROV position and orientation is complex, influenced by cable lengths, tensions, and thruster forces. This shifts the focus from pure forward kinematics to forward kinetostatics. As shown in Fig. 6, the forward kinetostatics

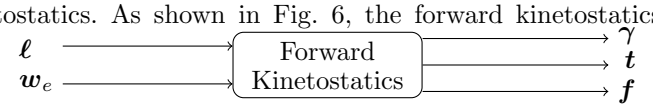

Fig. 6. Forward Kinetostatics

problem for the HCT-ROV has fewer equations ($m + 6$) than variables ($m + p + 6$), leading to a minimization problem. Its objective function is:

$$\begin{aligned} \min_{\boldsymbol{\gamma}_a} f(\boldsymbol{\gamma}_a, \boldsymbol{t}_a, \boldsymbol{f}_a) &= \|e(\boldsymbol{\gamma})\|_2^2 + \|W_c \boldsymbol{t}_a + W_t \boldsymbol{f}_a - \boldsymbol{w}_e\|_2^2 \\ \text{subject to:} \quad & t_{\min} \le t_i \le t_{\max}, \\ & f_{\min} \le f_i \le f_{\max} \end{aligned} \tag{10}$$

A nonlinear least-square solver can effectively resolve this problem. The goal is to determine the actual HCT-ROV pose $\boldsymbol{\gamma_a}$, considering desired cable lengths, while keeping cable tensions $\boldsymbol{t}_a$ and thruster forces $\boldsymbol{f}_a$ within specified limits. The minimization ensures error reduction and maintains the HCT-ROV in static equilibrium, adhering to the constraint $t_{\min} > 0$, for keeping the cables tensed.

2.4 Inverse Kinetostatics

The Inverse Kinetostatics of an HCT-ROV involves solving for the cable lengths, tensions, and thruster forces to reach a specified position and orientation with tensed cables.

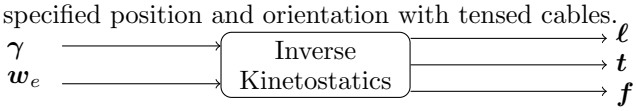

Fig. 7. Inverse kinetostatics

For the HCT-ROV prototype with $m = 4$ cables and $p = 8$ thrusters, solving for cable lengths is straightforward using the cable length equation (2). The challenge lies in determining cable tensions and thruster forces, requiring analysis of the static equilibrium equation (4). The latter forms an under-determined linear system ($m + p = 12 > 6$), leading to an optimization problem with bounds. Optimization can be performed using QP in MATLAB [2], formulated as:

$$\begin{aligned} [W_c \ W_t] \begin{bmatrix} \boldsymbol{t} \\ \boldsymbol{f} \end{bmatrix} &= [\boldsymbol{w}_e] \\ \text{subject to:} \quad & t_{\min} < t_i < t_{\max} \\ & f_{\min} < f_i < f_{\max} \end{aligned} \tag{11}$$

[2] `https://fr.mathworks.com/help/optim/ug/quadprog.html`

which can be rewritten as a linear system:

$$\begin{aligned} A\boldsymbol{x} &= b \\ \text{subject to:} \quad & x_{\min} < x_i < x_{\max}. \end{aligned} \tag{12}$$

A possible objective function consists in minimizing the weighted norm of $\boldsymbol{x}$ (comprising $\boldsymbol{t}$ and $\boldsymbol{f}$):

$$\begin{aligned} \min_{\boldsymbol{x}} \ & \frac{1}{2}\boldsymbol{x}^\top H \boldsymbol{x} \\ \text{subject to:} \quad & x_{\min} \leq x_i \leq x_{\max} \end{aligned} \tag{13}$$

In (13), the weight matrix H balances cable tensions and thruster forces contributions. Higher weights are assigned to thruster forces to prioritize solutions with lower thruster usage. This approach is consistent with control allocation strategies for overactuated systems, where managing actuator interactions is crucial Bodson (2002); Oppenheimer et al. (2006); Johansen and Fossen (2013). The HCT-ROV, with eight thrusters and four cables, exemplifies such system, guiding the allocation methodology via the QP controller.

3. EXPERIMENT AND RESULTS

The environment and vehicle parameters are based on the HCT-ROV prototype and the LIRMM laboratory setup for realistic simulation on MATLAB. Fig. 8 shows the LIRMM laboratory setup, where cable attachment points form a [3.20 3.34 4.42] (m) cuboid, within a one (m) deep pool.

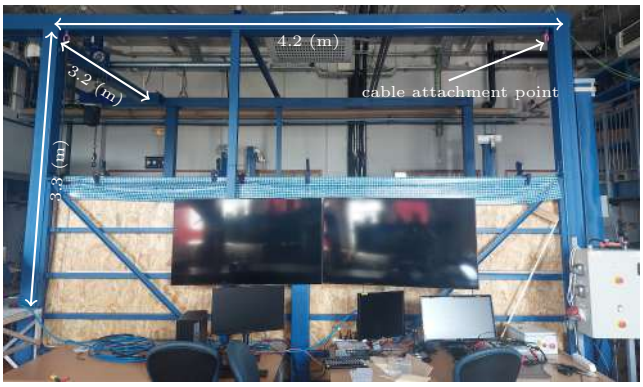

Fig. 8. LIRMM Laboratory setup

In the model, we neglected cable mass and elasticity as per Section 2.1, and assumed fixed attachment points. For dynamics, Coriolis and centripetal effects, damping coefficients, and external disturbances are disregarded. Assuming coinciding center of mass (COM) and center of buoyancy (COB) in the neutrally buoyant HCT-ROV, we exclude corresponding forces. The main role of the actuation system in the simulation is to counteract the vehicle inertia and the weight of the object it moves.

Vehicle parameters for the simulation derive from the real-life prototype and its CAD model, detailed in Table 1.

3.1 Experiment Procedure

Initially, a homing position outside the water was established at $[1.6, 2.211, 1, 0, 0, -0.322645]^\top$ (m and rad) in the pool center, considering the asymmetric design of the cables and z-axis rotation. For the HCT-ROV TP, a 5th-degree polynomial is used:

Table 1. Detailed parameters utilized in the simulation experiment, including vehicle mass, inertia, and actuation forces. Ranges

Parameter	Value
Vehicle mass outside water	76.35 kg
Vehicle mass inside water	0 kg (neutrally buoyant)
Object 1 mass inside water	15 kg
Object 2 mass inside water	250 kg
I_{xx}	13.14 kg.m^2
I_{yy}	12.91 kg.m^2
I_{zz}	16.72 kg.m^2
I_{xy}	0.09 kg.m^2
I_{xz}	-0.001 kg.m^2
I_{yz}	-0.08 kg.m^2
Thrust force range	-70 to 60 N
Cables tension range	0 to 1000 N

$$\boldsymbol{\gamma}(t) = a_0 + a_1 t + a_2 t^2 + a_3 t^3 + a_4 t^4 + a_5 t^5 \tag{14}$$

Velocity and acceleration profiles are derived from this polynomial first and second derivatives:

$$\dot{\boldsymbol{\gamma}}(t) = a_1 + 2a_2 t + 3a_3 t^2 + 4a_4 t^3 + 5a_5 t^4 \tag{15}$$

$$\ddot{\boldsymbol{\gamma}}(t) = 2a_2 + 6a_3 t + 12a_4 t^2 + 20a_5 t^3 \tag{16}$$

These equations compute the HCT-ROV desired trajectory, velocity, and acceleration for controlled movement. The unitary input approach normalizes time t to [0, 1] for simplifying coefficient calculations. Furthermore, the QP controller guarantees continuous solutions for the cable tension and thruster force over time, resulting in smooth transitions along the TP.

3.2 Experiment Scenario Breakdown

The experiment goal is to retrieve an object from 1 (m) depth and return it to the homing position under four conditions, testing HCT-ROV capabilities:

(1) **ROV Only with Light Object**: Uses thrusters for a 15 (kg) object, assessing ROV load handling and TP.
(2) **ROV Only with Heavy Object**: Employs thrusters for a 250 (kg) object, testing ROV heavy load limits.
(3) **HCT-ROV with Light Object**: Demonstrates control allocation efficacy with a 15 (kg) load and reduced thruster use.
(4) **HCT-ROV with Heavy Object**: Utilizes the full HCT-ROV system for a 250 (kg) object, showcasing hybrid actuation system enhanced lifting capabilities.

3.3 Simulation Results

ROV Only with Light Object The ROV successfully transported a 15 (kg) object, reaching the goal at $T = 40$ (s) and returning by $T = 80$ (s), as Fig. 9 shows. Thruster analysis Fig. 10 reveals limitations in lifting capabilities, with thrusters nearing their capacity 60 (N). Note that, the four horizontal thrusters (1,2,3,4) maintain a zero thrust force during the mission, while the four vertical thrusters (5,6,7,8) exhibit varying yet equal force for lifting the object.

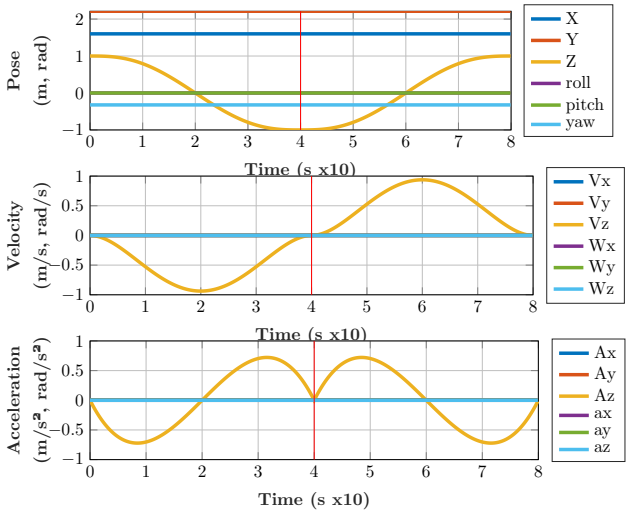

Fig. 9. ROV Only with Light Object: velocity and acceleration profile. Illustrating the TP success. $T = 40\,(\mathrm{s})$: Goal pose reached, $T = 80\,(\mathrm{s})$: Home pose reached with payload.

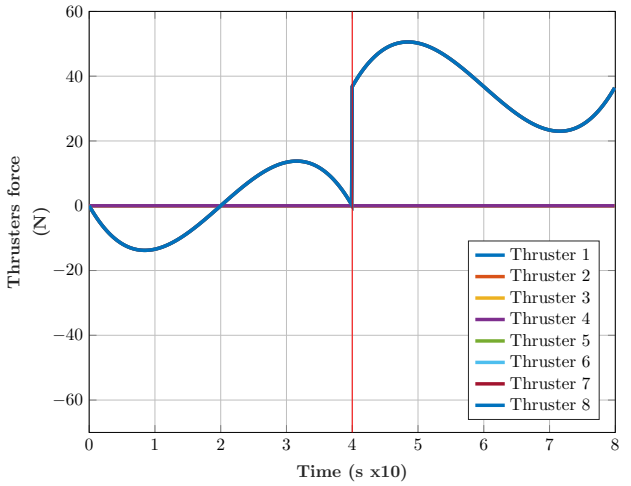

Fig. 10. Thruster forces of ROV Only with Light Object. Illustrating ROV limitations in transporting payloads as the thrusters are nearing their capacity [-70:60] (N) for the 15 (kg) payload starting from $T = 40\,(\mathrm{s})$.

ROV Only with Heavy Object This test Fig. 11 and 12 indicated ROV inability to lift a 250 (kg) load, failing the task.

HCT-ROV with Light Object Comparing Fig. 10 with Fig. 13 shows a 72.73% thrust force reduction for the 15 (kg) load with HCT-ROV, indicating control allocation success.

HCT-ROV with Heavy Object Comparing Fig. 12 with Fig. 14, the HCT-ROV successfully managed a 250 (kg) payload, highlighting the system lifting capabilities and control allocation success. Horizontal thrusters played a key role in maintaining stability and control.

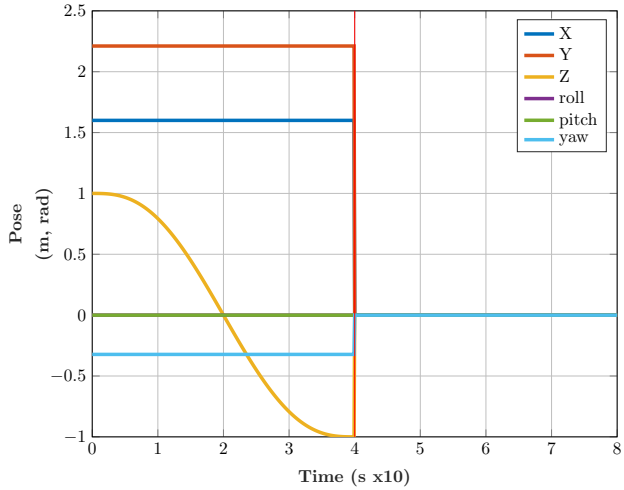

Fig. 11. Pose profile of ROV Only with Heavy Object. Illustrating ROV failure in moving the 250 (kg) payload.

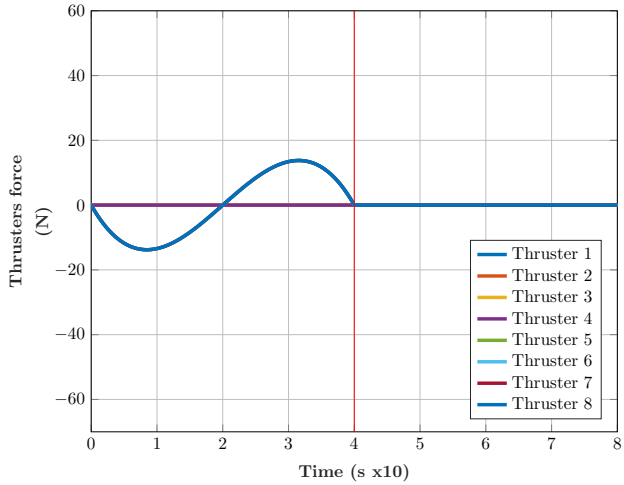

Fig. 12. Thruster forces of ROV Only with Heavy Object.

4. CONCLUSION AND FUTURE WORK

The HCT-ROV prototype demonstrated its potential in simulation trials, validating the control law and control allocation using kinetostatic modeling and QP methodology. These trials tested the vehicle with various payloads, focusing on:

(1) Validating TP and simulation effectiveness.
(2) Showcasing ROV limitations with heavy loads.
(3) Proving control allocation efficacy in reducing thruster force requirements.
(4) Demonstrating the hybrid actuation system superiority in lift capability over conventional ROV.

The vehicle behavior and the output graphs across simulations substantiate these claims.

4.1 Future Work

Forward Kinetostatics Validation: The forward kinetostatics control law, theoretically able to determine the vehicle pose using cable actuation system sensors (encoders

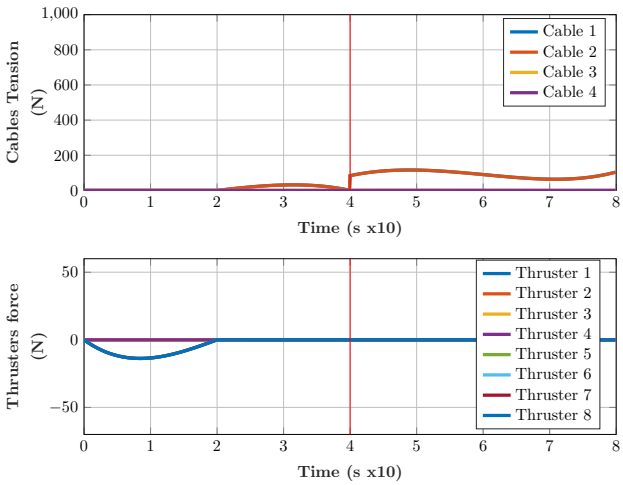

Fig. 13. Cable and thruster forces of HCT-ROV with Light Object. Illustrating the desired thrust reduction by 72.73% compared to Fig. 10, showing the success of control allocation by QP.

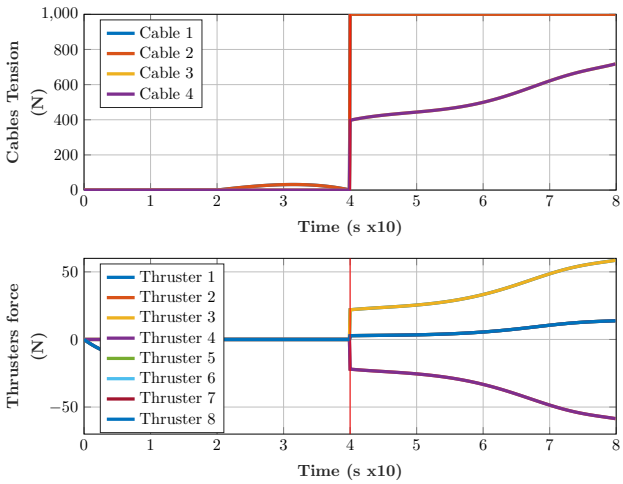

Fig. 14. HCT-ROV with Heavy Object: Cables and Thrusters force. Illustrating the enhanced lift capabilities of HCT-ROV by lifting the 250 (kg) payload the ROV failed to lift in Fig. 12

and load cells), remains to be validated against a DVL-integrated HCT-ROV for accuracy comparison.

Real-world Scenario Testing: With ongoing mechanical adjustments at LIRMM, the next step is real-life testing of the HCT-ROV, mirroring simulation experiments. Post-validation, the prototype will face external disturbances like artificial waves to assess its robustness.

ACKNOWLEDGEMENTS

This research was partially funded by the European Union - NextGenerationEU and by the Ministry of University and Research (MUR), National Recovery and Resilience Plan (NRRP), Mission 4, Component 2, Investment 1.5, project "RAISE - Robotics and AI for Socio-economic Empowerment" (ECS00000035). Enrico Simetti and Youssef Attia are part of RAISE personnel.

REFERENCES

Abbasnejad, G. and Carricato, M. (2015). Direct geometrico-static problem of underconstrained cable-driven parallel robots with n cables. *IEEE Transactions on Robotics*, 31(2), 468–478. doi:10.1109/TRO.2015.2393173.

Bodson, M. (2002). Evaluation of optimization methods for control allocation. *Journal of Guidance, Control, and Dynamics*, 25(4), 703–711. doi:10.2514/2.4937.

Carricato, M. and Merlet, J.P. (2013). Stability analysis of underconstrained cable-driven parallel robots. *IEEE Transactions on Robotics*, 29(1), 288–296. doi:10.1109/TRO.2012.2217795.

Cieślak, P., Simoni, R., Rodríguez, P.R., and Youakim, D. (2020). Practical formulation of obstacle avoidance in the Task-Priority framework for use in robotic inspection and intervention scenarios. *Robotics and Autonomous Systems*, 124, 103396. doi:10.1016/j.robot.2019.103396.

El-Ghazaly, G., Gouttefarde, M., and Creuze, V. (2015). Hybrid cable-thruster actuated underwater vehicle-manipulator systems: A study on force capabilities. In *2015 IEEE/RSJ International Conference on Intelligent Robots and Systems (IROS)*, 1672–1678. doi:10.1109/IROS.2015.7353592.

Gouttefarde, M. and Bruckmann, T. (2022). Cable-driven parallel robots. In *Encyclopedia of Robotics*, 1–14. Springer Berlin Heidelberg. doi:10.1007/978-3-642-41610-1_149-1.

Gouttefarde, M., Rodriguez, M., Barrelet, C., Hervé, P.E., Creuze, V., Gorrotxategi, J., Oyarzabal, A., Culla, D., Sallé, D., Tempier, O., Ferrari, N., Chaumont, M., and Subsol, G. (2023). The robotic seabed cleaning platform: An underwater cable-driven parallel robot for marine litter removal. In *Cable-Driven Parallel Robots*, 430–441. Springer Nature Switzerland, Cham.

Idà, E., Bruckmann, T., and Carricato, M. (2019). Rest-to-rest trajectory planning for underactuated cable-driven parallel robots. *IEEE Transactions on Robotics*, 35(6), 1338–1351. doi:10.1109/TRO.2019.2931483.

Johansen, T.A. and Fossen, T.I. (2013). Control allocation—a survey. *Automatica*, 49(5), 1087–1103. doi:10.1016/j.automatica.2013.01.035.

Mishra, U.A. and Caro, S. (2021). Unsupervised neural network based forward kinematics for cable-driven parallel robots with elastic cables. In *Cable-Driven Parallel Robots*, 63–76. Springer International Publishing, Cham.

Oppenheimer, M.W., Doman, D.B., and Bolender, M.A. (2006). Control allocation for over-actuated systems. In *2006 14th Mediterranean Conference on Control and Automation*, 1–6. doi:10.1109/MED.2006.328750.

Sacchi, N., Simetti, E., Antonelli, G., Indiveri, G., Creuze, V., and Gouttefarde, M. (2022). Analysis of hybrid cable-thruster actuated rov in heavy lifting interventions. In *2022 IEEE/RSJ International Conference on Intelligent Robots and Systems (IROS)*, 8430–8435. doi:10.1109/IROS47612.2022.9981861.

Simetti, E. (2020). Autonomous Underwater intervention. *Curr Robot Rep*, 1(3), 117–122. doi:10.1007/s43154-020-00012-7.